A controllable spin prism

J. Phys.: Condens. Matter **21** (2009) 026016 (9pp) doi:10.1088/0953-8984/21/2/026016

A controllable spin prism

T Hakioğlu

Department of Physics, Bilkent University, 06800 Ankara, Turkey
and
UNAM Material Science and Nanotechnology Institute, Bilkent University, 06800 Ankara, Turkey

Received 10 June 2008, in final form 3 November 2008
Published 10 December 2008
Online at stacks.iop.org/JPhysCM/21/026016

Abstract
Based on Khodas *et al* (2004 *Phys. Rev. Lett.* **92** 086602), we propose a device acting like a controllable prism for an incident spin. The device is a large quantum well where Rashba and Dresselhaus spin–orbit interactions are present and controlled by the plunger gate potential, the electric field and the barrier height. A totally destructive interference can be manipulated externally between the Rashba and Dresselhaus couplings. The spin-dependent transmission/reflection amplitudes are calculated as the control parameters are changed. The device operates as a spin prism/converter/filter in different regimes and may stimulate research in promising directions in spintronics in analogy with linear optics.

(Some figures in this article are in colour only in the electronic version)

The controllability of spin has been of crucial importance in the development of spintronics device physics since the proposal of Datta and Das [1] in the 1990s. Although the Datta–Das spin FET has not been experimentally realized yet, the research on spintronics devices based on nonmagnetic and magnetic semiconductors is continuing [2]. In most of the theoretical and experimental works the Rashba (R) spin–orbit coupling (SOC) [3] is the basic mechanism to manipulate the electron spin [4] and in some others Rashba and Dresselhaus [5] (D) SOCs are considered [6, 7]. Some other proposals have been made on SOC-based devices in larger quantum circuits utilizing additional effects such as the Aharonov–Bohm and the Aharonov–Casher effects [8]. These theoretical and experimental proposals have been discussed in many reviews [9].

Recently, a mechanism has been suggested corresponding to a spin analog of the optical Snell's law [10]. The idea is the splitting of an incident spin-1/2 state into two angularly resolved spin-dependent components. In that work, the interface of two nonmagnetic semiconductors with different SOCs (only Rashba type was considered) in the conduction band was used for creating a spin-dependent refraction. The ideas in [10] found many applications, among which are the spin-dependent negative refraction [11] and perfect spin filtering across a semiconductor tunnel barrier [12]. In this paper we extend this idea of spin-dependent refraction to a theoretical device with a large number of control parameters and demonstrate that the range of the diffraction angles between the propagating spin–orbit modes can be controlled externally. We identify three distinct types of propagation at large angles of incidence. Additionally, including the Dresselhaus SOC is a 'must' in many zinc blende structures [13–15]. In the presence of both SOC contributions, it is shown that a totally destructive interference can be externally manipulated between the Rashba and the Dresselhaus contributions.

One of the main result of this simple work is that the control parameters can be tuned to obtain a rich number of configurations such as the total reflection of both spin–orbit states, the reflection of one and the transmission of the other, the transmission of both as well as a nontrivial spin-independent diffraction. The other results are concerned with the controllability of the spin-dependent transmission and reflection amplitudes.

The model. We consider a simple quantum mechanical system as shown in figure 1 consisting of a large quantum well (QW) in the region $|x| \leqslant b$ between two strong spin-independent potential barriers at $b \leqslant |x| \leqslant a$. The R&D spin–orbit couplings are effective within the QW, and the former is tunable by an electric field E_z in the z direction. The system is translationally invariant in the y direction. The SOCs and E_z are effective only within the QW. The electrons from the, say left, reservoir impinge on the interface $x = -a$ with their wavevectors $\vec{Q} = (Q_x, Q_y)$. Here it is demonstrated that, despite its simplicity, scattering through this structure is quite rich in physics due to the effects of the control parameters E_z, the barrier height V_0, the plunger gate potential V_P as well as the parameters of incidence, i.e. the

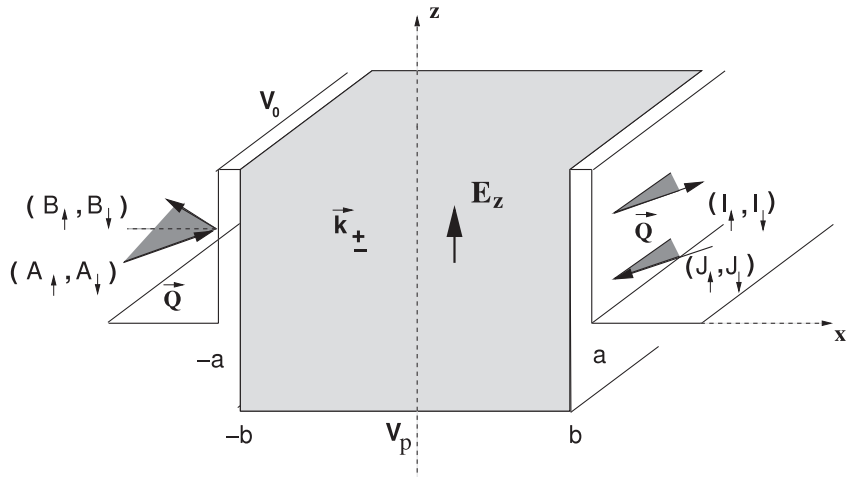

Figure 1. The QW model considered. The R&D spin–orbit interactions and the electric field along the z direction are confined within the well $-b \leqslant x \leqslant b$ (shaded area) and zero outside. The interfaces with the potential barriers at $x = \pm a$ and $\pm b$ are considered to be spin-independent. The spin dependence of the waves are described by $(A_\uparrow, A_\downarrow)$ for the left incident, $(B_\uparrow, B_\downarrow)$ for the reflected, $(I_\uparrow, I_\downarrow)$ for the transmitted and $(J_\uparrow, J_\downarrow)$ for the right incident waves. Note that we only consider left incidence and $(J_\uparrow, J_\downarrow) = 0$.

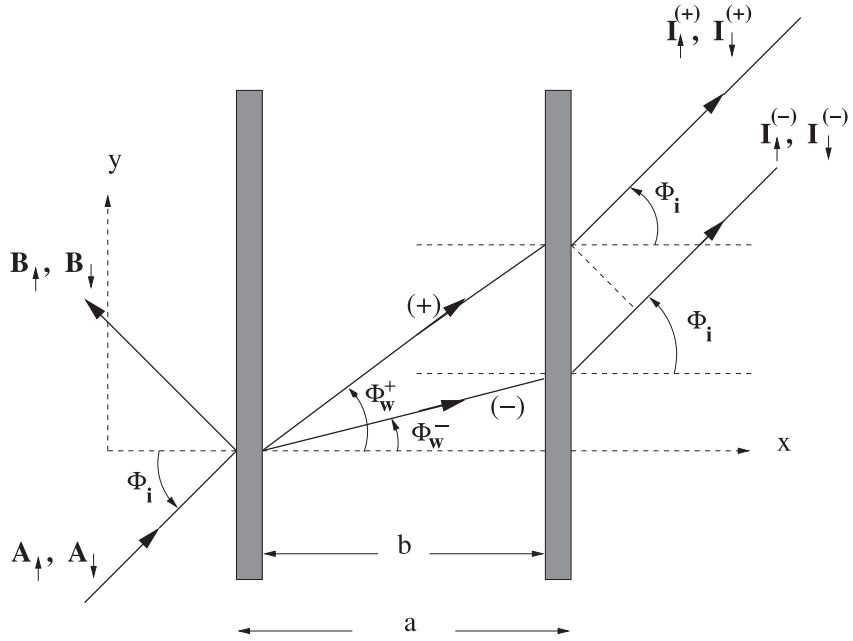

Figure 2. The diffraction and the reflection of the incident wave in the QW (looking down in the negative z direction in figure 1). The angle of incidence is ϕ_i and the angles of diffraction within the QW are $\phi_w^{(\pm)}$ corresponding to both $+$ and $-$ modes. Note the decomposition of the transmission amplitudes $I_\uparrow$ and $I_\downarrow$ in $I^{(+)} = I_\uparrow^{(+)} + I_\downarrow^{(+)}$ in the transmission of the $+$ spin–orbit branch and $I^{(-)} = I_\uparrow^{(-)} + I_\downarrow^{(-)}$ in the transmission of the $-$ spin–orbit branch.

energy $E = \hbar^2 Q^2/(2m^*) < V_0$, the angle of incidence $\phi_i = \tan^{-1}(Q_y/Q_x)$ within the xy plane and the initial spin configuration of the electrons. In this paper, we assume zero-conductance conditions and an additional tunable source–drain potential is not considered.

The device is represented by a 4×4 unitary S-matrix:

$$\begin{pmatrix} B_\uparrow \\ B_\downarrow \\ I_\uparrow \\ I_\downarrow \end{pmatrix} = \mathbf{S} \begin{pmatrix} A_\uparrow \\ A_\downarrow \\ J_\uparrow \\ J_\downarrow \end{pmatrix} \tag{1}$$

where $Q = |\vec{Q}|$ and in a certain incident spin state. Here $A_\uparrow, A_\downarrow$ $(B_\uparrow, B_\downarrow)$ are the partial spin amplitudes on the Bloch sphere of the left incident (reflected) electron and $I_\uparrow, I_\downarrow$ $(J_\uparrow, J_\downarrow)$ are those of the right incident (reflected) electron. The electron wavefunctions on the left and right are given by

$$\Psi(\vec{r}) = \sum_{\sigma=(\uparrow,\downarrow)} \left[X_\sigma e^{i\vec{Q}\cdot\vec{r}} + Y_\sigma e^{i\bar{\vec{Q}}\cdot\vec{r}} \right] |\sigma\rangle \tag{2}$$

where $\bar{\vec{Q}} = (-Q_x, Q_y)$. We assume that the electrons are incident from the left and the amplitudes of the right incidence

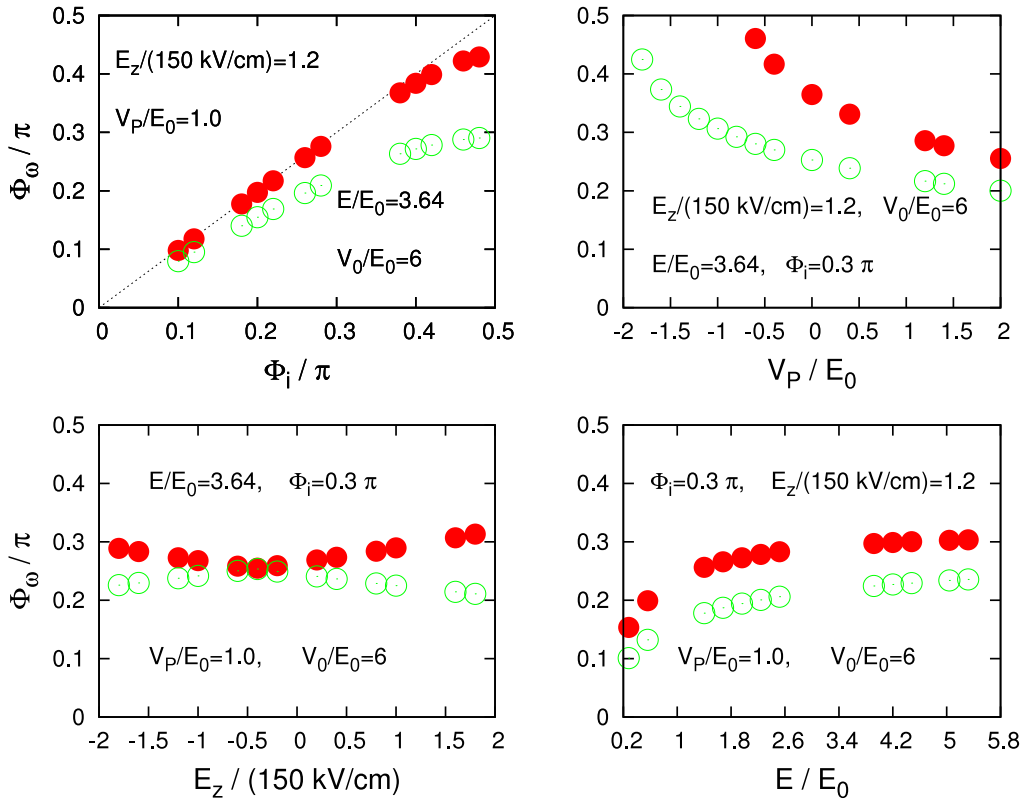

Figure 3. (Color online) The solution of equation (2) for $\phi_w^{(+)}$ (red solid circles) and $\phi_w^{(-)}$ (green hollow circles) as ϕ_i, E_z, V_P and E are varied. The solutions yield total propagation of the QW modes. Dashed lines in $\phi_w^{(\pm)}$ correspond to the 45° line.

$(J_\uparrow, J_\downarrow)$ are considered to be zero. Under this condition the coefficients $(I_\uparrow, I_\downarrow)$ will be termed as the spin-dependent transmission coefficients. For the incident and reflected waves on the left barrier we have $X_\sigma = A_\sigma, Y = B_\sigma$ and for the transmitted one $X_\sigma = I_\sigma$ with $Y_\sigma = J_\sigma = 0$. The wavefunction within the spin-independent barriers ($b \leqslant |x| \leqslant a$) is exponential whereas, in the QW ($|x| \leqslant b$), it is described by a superposition of the eigenstates of the Hamiltonian written in the spin basis ($|\uparrow\rangle$ $|\downarrow\rangle$):

$$H_{\rm QW} = \frac{\hbar^2 k^2}{2m^*} + \begin{pmatrix} 0 & -{\rm i}\alpha_{\rm R} k_- + \alpha_{\rm D} k_+ \\ {\rm i}\alpha_{\rm R}^* k_+ + \alpha_{\rm D}^* k_- & 0 \end{pmatrix} + eV_{\rm P} \tag{3}$$

where $m^* = 0.067 m_{\rm e}$, where $m_{\rm e}$ is the electron's rest mass. The R&D SOCs are given by $\alpha_{\rm R} = r_{41}^{6c6c} E_z$ and $\alpha_{\rm D} = -b_{41}^{6c6c} \langle k_z^2 \rangle$ for the conduction band as given, for instance, in [14], by the band theory estimates in the proper growth direction with $r_{41}^{6c6c} \simeq 117e$ Å^2 and $b_{41}^{6c6c} = 27.2$ eV Å^3 for InAs and $r_{41}^{6c6c} \simeq 523e$ Å^2 and $b_{41}^{6c6c} = 760$ eV Å^3 for InSb. In this work we use the InAs parameters. Considering a sample thickness in the z direction $W \simeq 60$ Å we have $\langle k_z^2 \rangle \simeq (\pi/W)^2 = 2.7 \times 10^{-3}$ Å^{-2}. The wavefunction within the QW (i.e. $|x| \leqslant b$) is then

$$\Psi_{\rm QW}(\vec{r}) = \sum_{\lambda=(+,-)} \left[E_\lambda {\rm e}^{{\rm i}\vec{k}^{(\lambda)}\cdot\vec{r}} + F_\lambda {\rm e}^{{\rm i}\bar{\vec{k}}^{(\lambda)}\cdot\vec{r}} \right] |\lambda\rangle \tag{4}$$

where $\vec{k}^{(\pm)} = (k_x^{(\pm)}, k_y^{(\pm)})$, $\bar{\vec{k}}^{(\pm)} = (-k_x^{(\pm)}, k_y^{(\pm)})$ and E_λ, F_λ are the amplitudes of the right moving and the left moving waves with $\lambda = \pm$ corresponding to the index of the eigenstates of equation (3) given by

$$|\lambda, \vec{k}^{(\lambda)}\rangle = \left(|\uparrow, \vec{k}^{(\lambda)}\rangle + \lambda {\rm e}^{-{\rm i}\phi_{\rm so}^{(\lambda)}} |\downarrow, \vec{k}^{(\lambda)}\rangle \right) \Big/ \sqrt{2}. \tag{5}$$

The wavevectors $\vec{k}^{(\pm)}$ of the spin–orbit modes as well as the phase $\phi_{\rm so}^{(\lambda)}$ within the QW have to be determined by the boundary conditions at the interfaces (see equation (6) below).

The refraction of the incident electrons. The time-independent quantum states in the QW, where R&D spin–orbit couplings are present, are represented as superpositions of standing waves with wavevectors $\vec{k}^{(\pm)}$. Due to the translational invariance along the y direction, the wavevector in this direction is conserved along the interfaces, i.e. $Q_y = k_y^{(+)} = k_y^{(-)}$. The spin–orbit modes that propagate through the well are then determined by

$$\begin{aligned} E &= \frac{\hbar^2 Q^2}{2m^*} = \frac{\hbar^2 (k^{(\pm)})^2}{2m^*} \pm |\alpha_{\rm so}(\phi_w^{(\pm)})| k^{(\pm)} + eV_{\rm P} \\ \alpha_{\rm so}(\phi_w^{(\pm)}) &= {\rm e}^{{\rm i}\phi_{\rm so}^{(\pm)}} \sqrt{(\alpha_{\rm R}^2 + \alpha_{\rm D}^2) - 2\alpha_{\rm R}\alpha_{\rm D} \sin 2\phi_w^{(\pm)}} \\ \sin \phi_w^{(\pm)} &= Q_y / k^{(\pm)} \end{aligned} \tag{6}$$

where $e = -|e|$ is the electron charge, $\alpha_{\rm so}(\phi_w^{(\pm)})$ is the combined R&D-type SOCs given by the coupling strengths $\alpha_{\rm R}$ and $\alpha_{\rm D}$, respectively [14, 15], $k^{(\pm)} = |\vec{k}^{(\pm)}|$ and $0 \leqslant \phi_w^{(\pm)} \leqslant \pi/2$ are the magnitudes of the wavevectors and the angles of diffraction, respectively, within the QW. Equation (6) solely

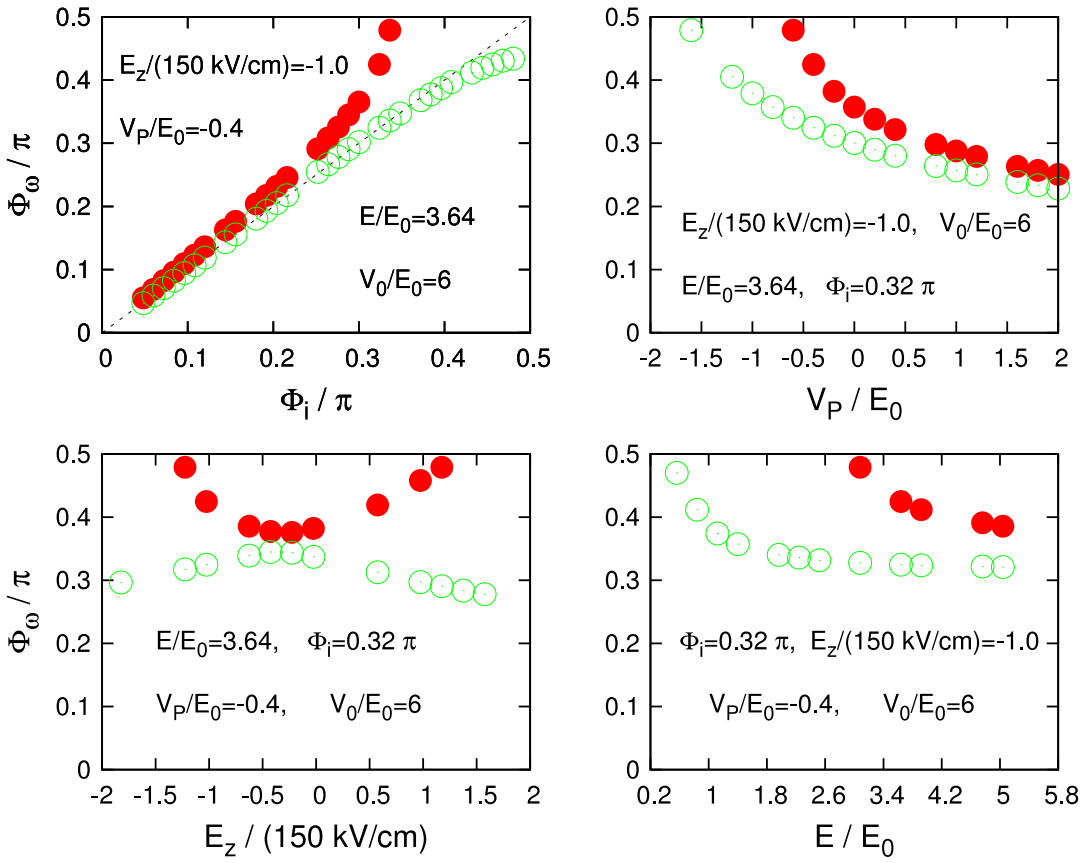

Figure 4. (Color online) Same as in figure 3 for $V_{\rm P} = 0$. The solutions yield propagation of the $-$ mode and total reflection of the $+$ mode for large ϕ_i.

depends on the translational invariance along the y direction and the energy conservation which can be found independently from the reflection and transmission (TR) amplitudes. We therefore solve these equations to determine the angles of diffraction within the QW which then enter in the calculation of the TR amplitudes (which we consider later below). The first expression in (6) is the energy conservation, the second is the complex SOC including the Rashba ($\alpha_{\rm R}$) and the Dresselhaus ($\alpha_{\rm D}$) contributions, and the third one is the angle of diffraction within the QW based on the translational invariance in the y direction. The phase of the complex spin–orbit coupling constant $\alpha_{\rm so}$ described by the second equation in (6) is determined by

$$\tan\phi_{\rm so}^{(\pm)} = \frac{-\alpha_{\rm R}/\alpha_{\rm D} + \tan\phi_w^{(\pm)}}{-(\alpha_{\rm R}/\alpha_{\rm D})\tan\phi_w^{(\pm)} + 1}. \qquad (7)$$

In our calculations, all lengths are scaled by Q_0 and all energies by $E_0 = \hbar^2 Q_0^2/(2m^*)$, where Q_0 is defined to be the reference Fermi wavevector of free electrons in 2D with concentration $n_{\rm e} \simeq 10^{11}$ cm^{-2}. For these values $Q_0 = \sqrt{4\pi n_{\rm e}} \simeq 0.01$ Å^{-1} and the corresponding energy reference scale is $E_0 \simeq 6$ meV. For an electric field $E_z = 150$ kV cm^{-1} (which we consider as the reference electric field by which E_z is scaled), and for $|\vec{Q}| = Q_0$, we find that the R&D spin–orbit energy scales are $E_{\rm R} = \alpha_{\rm R} Q_0 \simeq 1.7$ and $E_{\rm D} = \alpha_{\rm D} Q_0 \simeq -0.76$ meV, which are considerably smaller compared to the corresponding energy scale E_0. The dimensions of the QW in the x direction are considered to be $2a = 70$ and $2b = 60$ nm. The barrier height is fixed at $V_0/E_0 = 6$. In this work, the tunable parameters are varied in the range $0 \leqslant E/E_0 \leqslant 5.8$, $-2.0 \leqslant E_z/(150\ \text{kV cm}^{-1}) \leqslant 2.0$ and $-2.0 \leqslant V_{\rm P}/E_0 \leqslant 2.0$. Despite the fact that the energy scales of the R&D SOCs are small with respect to the energy of the incident electrons, its effects on the spin-dependent refraction and the transmission/reflection amplitudes are nonnegligible.

The wavevectors $\vec{k}^{(\pm)}$, the diffraction angles $\phi_w^{(\pm)}$ and the spin–orbit phase $\phi_{\rm so}^{(\pm)}$ are found by the solution of the nonlinear equations in (6). The resulting modes $|\lambda, \vec{k}^{(\lambda)}\rangle$, $(\lambda = \pm)$ described by equation (5) are *not orthogonal* as a result of $k^{(+)} \neq k^{(-)}$ and $\phi_w^{(+)} \neq \phi_w^{(-)}$. The initial spin state is then split into a superposition of the modes in equation (5), with each mode exposed to a different SOC strength self-consistently determined by equation (6) and yielding different propagation directions as schematically shown in figure 2. Based on [10], we call this device a *controllable spin prism*. What makes this proposal interesting is that the diffraction within the QW and hence the transmission through the device can be determined not only by the conditions of incidence fixed by ϕ_i, E and the initial spin configuration, but also precisely controlled externally by E_z, $V_{\rm P}$ and V_0. In particular, the diffraction of the spin–orbit modes within the QW is controllable using $V_{\rm P}$, i.e. for a given set of other control parameters, both modes propagate for sufficiently large $0 < V_{\rm P}$ (see figure 3), the $+$ mode is totally reflected for small $V_{\rm P}$ and large ϕ_i (figure 4) and both modes are totally reflected for large $V_{\rm P} < 0$ and large

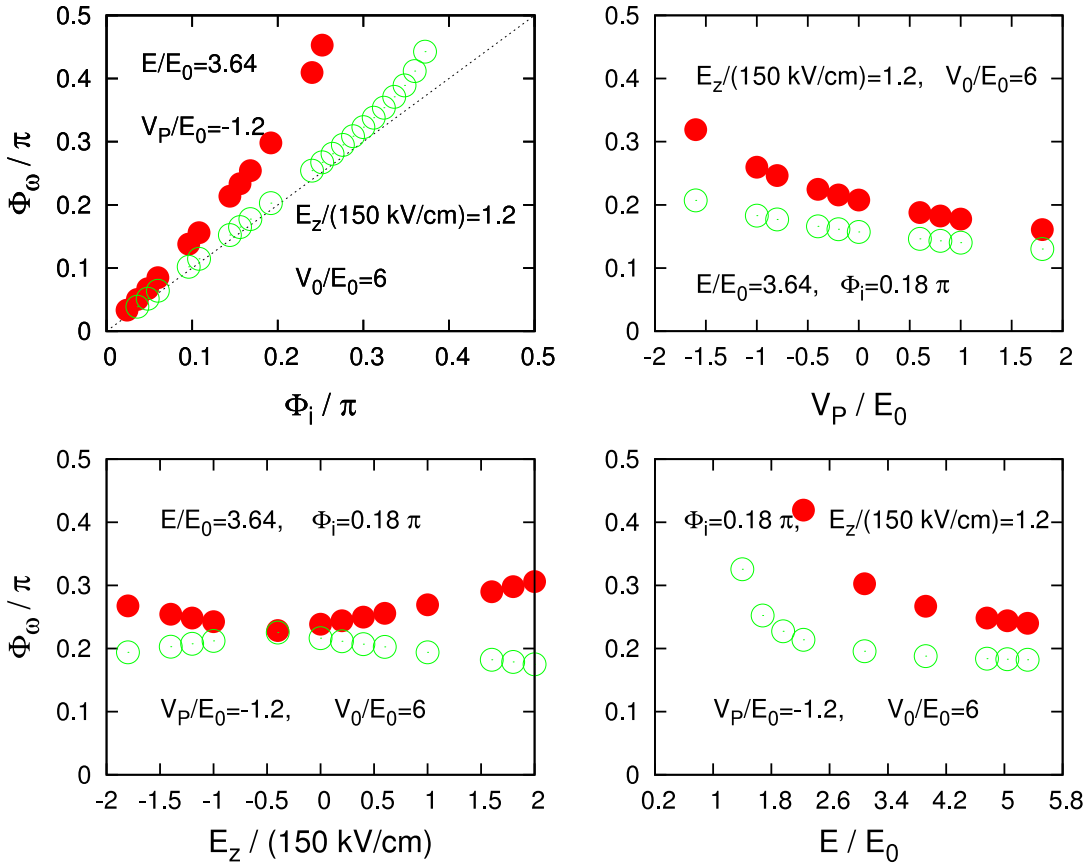

Figure 5. (Color online) Same as in figure 3 for $V_P/E_0 = -1.2$. The solutions yield total reflection of both modes for large ϕ_i.

ϕ_i (figure 5). We also observe that, for small E and V_P, the two solutions are considerably different and for large values of these parameters they converge to a single solution (see plots of ϕ_i versus V_P and ϕ_i versus E in figures 3–5).

An interesting consequence of the simultaneous presence of the R&D couplings is in the dependence of α_{so} on the diffraction angles $\phi_w^{(\pm)}$, implying that the different spin–orbit modes propagating within the QW are subjected to different SOCs. At a fixed value of $E_z < 0$ corresponding to $\alpha_R = \alpha_D \neq 0$, the solutions can be forced to yield a completely destructive interference between the Rashba and the Dresselhaus couplings, i.e. $|\alpha_{so}| = 0$. This value can be found to be $E_z/(150\ \text{kV cm}^{-1}) \simeq -0.42$ by using the SOC strengths for InAs specified below equation (3). Inspecting equation (6) it can be seen that this particular configuration is obtained when ϕ_i, V_P and E are related by

$$\sin\phi_i = \sqrt{\frac{E + |e|V_P}{2E}}. \tag{8}$$

As the result, two spin–orbit modes are forced to diffract independently from spin at $\phi_w^{(\pm)} = \pi/4$. In this case, the incident spin state transmits through the device unchanged. This feature is present in the $\phi_w^{(\pm)}$ versus E_z plots in figures 3 and 5 where the two solutions meet. For the E and V_P values used, those incidence angles supporting spin-independent transmission, i.e. $|\alpha_{so}| = 0$, are $\phi_i/\pi \simeq 0.29$ in figure 3 and $\phi_i/\pi \simeq 0.19$ in figure 5. Other applications of the condition $\alpha_R = \alpha_D$ have been studied previously considering normal incidence [6]. On the other hand, when ϕ_i, V_P and E do not respect equation (8), the SOC can still be minimized at a nonzero value and the interference between R&D contributions is partially destructive, yielding a small splitting $\phi_w^{(+)} - \phi_w^{(-)} \neq 0$ as shown in the $\phi_w^{(\pm)}$ versus E_z plots in figure 4. From equation (6) we also conclude that, for $E - eV_P \simeq 0$ and positive, the + mode is totally reflected for nonzero angles of incidence. The − mode is transmitted respecting $\sin\phi_w^{(-)} \simeq \sqrt{eV_P}\sin\phi_i/|\alpha_{so}(\phi_w^{(-)})|$. For large and negative V_P or small α_{so} this mode is also totally reflected. In this respect, a variety of spin selective transmissions can be managed even at small angles of incidence.

The relative optical phase. Another consequence of $\phi_w^{(+)} \neq \phi_w^{(-)}$ and $k^{(+)} \neq k^{(-)}$ is that there is a significant relative optical phase difference between the + and the − modes. In the geometry of figure 2 this can be easily found to be

$$\frac{\Delta\phi_{opt}}{Qb} = \left[\frac{k^{(+)}/Q}{\cos\phi_w^{(+)}} - \frac{k^{(-)}/Q}{\cos\phi_w^{(-)}}\right] - \sin\phi_i[\tan\phi_w^{(+)} - \tan\phi_w^{(-)}] \tag{9}$$

where the terms proportional to $\sin\phi_i$ are the contributions from the transmitted region on the right, and the other terms are those within the QW. As shown in figure 6, $\Delta\phi_{opt}$ can be very large for large angles of incidence and a significant interference can be observed between the partial amplitudes of

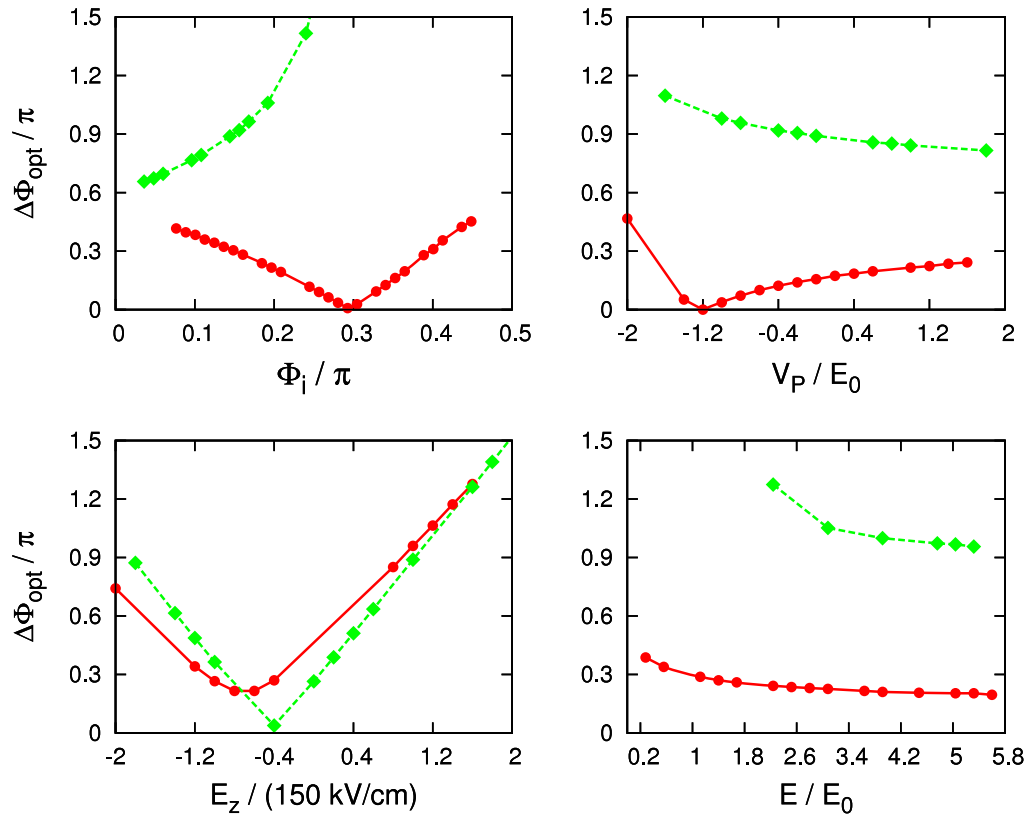

Figure 6. (Color online) $\Delta\phi_{\rm opt}$ as ϕ_i, E_z, $V_{\rm P}$ and E are varied for two different parameter sets. The parameters in each plot (excluding the variable on the horizontal axis) are $V_{\rm P}/E_0 = 1$, $E/E_0 = 3.64$, $\phi_i = 0.18\pi$, $E_z/(150\ {\rm kV\ cm^{-1}}) = -0.8$ for the red circles, and $V_{\rm P}/E_0 = -1.2$, $E/E_0 = 3.64$, $\phi_i = 0.18\pi$, $E_z/(150\ {\rm kV\ cm^{-1}}) = 1.2$ for the green diamonds.

the transmitted state. The two different parameter sets used are indicated in the figure captions. The data indicated by the green diamonds refer to the same parameters used in figure 5. The point corresponding to $\alpha_{\rm R} = \alpha_{\rm D}$ at $E_z/(150\ {\rm kV\ cm^{-1}}) \simeq -0.42$ in the ϕ_w versus E_z in that figure yields $\Delta\phi_{\rm opt} = 0$. In this case the two spin–orbit modes have the same wavevector and the diffraction angle, hence they share identical optical paths. The other data corresponding to the red circles are chosen such that equation (8) is satisfied at two different points, the first being at $V_{\rm P}/E_0 = 1$, $\phi_i = 0.3\pi$, as shown in the upper left plot, and the second being at $V_{\rm P}/E_0 = -1.2$, $\phi_i = 0.18\pi$, as shown in the upper right one. All zeros of the optical phase again correspond to the solutions of (6) where $|\alpha_{\rm so}| = 0$.

The transmission and the reflection amplitudes. The diffraction angles $\phi_w^{(\pm)}$ found by the solution of equation (6) affect the scattering states via the boundary conditions which are encoded in the TR amplitudes $(B_\uparrow, B_\downarrow, I_\uparrow, I_\downarrow)$. The wavefunction and the spin-dependent current are conserved across the interfaces via [10]:

$$\Psi(\vec{r})|_n^{n+1} = 0, \qquad \left[\frac{{\rm i}\hbar\partial_x}{m^*} + \alpha_{\rm so}(\vec{r})\sigma_y\right]\Psi(\vec{r})\Big|_n^{n+1} = 0 \quad (10)$$

where n and $n+1$ represent two consecutive media along the x direction, as shown in figure 1, and $\Psi(\vec{r})$ denotes the wavefunctions of the two neighboring media. We consider that the potential barriers at $b \leqslant |x| \leqslant a$ are spin-independent and the R&D SOCs are nonzero only within the QW between $|x| \leqslant b$. Satisfying equation (10) and multiplying the transmission matrices of each region, and converting the T-matrix into a unitary S-matrix the TR amplitudes $I_\uparrow, I_\downarrow, B_\uparrow, B_\downarrow$ in equation (1) are obtained. The TR amplitudes are examined in figure 7 as a function of the parameters of incidence ϕ_i, E for fixed $E_z, V_{\rm P}, V_0$ and $A_\uparrow = 1, A_\downarrow = 0$. The plots, starting from the top left corner, respect the order in the counter-clockwise sense with $B_\uparrow$: the reflected up spin amplitude, $B_\downarrow$: the reflected down spin amplitude, $I_\downarrow = I_\downarrow^{(+)} + I_\downarrow^{(-)}$: the transmitted down spin amplitude including the contributions of both partial amplitudes $I_\downarrow^{(\pm)}$ and, $I_\uparrow = I_\uparrow^{(+)} + I_\uparrow^{(-)}$: the transmitted up spin amplitude again including the contribution of both partial amplitudes $I_\uparrow^{(\pm)}$. This particular decomposition of the partial amplitudes is used for the purpose of identifying the spin preserving and flipping processes. In the plots, $B_\uparrow, B_\downarrow, I_\uparrow$, and $I_\downarrow$ include many resonant features identified within the range of initial parameters $5.4 \leqslant E/E_0 \leqslant 5.8$ and $0.25 \leqslant \phi_i/\pi \leqslant 0.35$ at $V_{\rm P}/E_0 = 0.4$ and $E_z/(150\ {\rm kV\ cm^{-1}}) = 1.6$.

In figure 7 a variety of different processes is present such as strongly spin-preserving or spin-flipping transmissions and reflections at different values of the incidence and the control parameters. In this variety, we will only examine below strongly spin-flipping transitions. In particular, sharp resonances are observed in figure 7 at ($\phi_i/\pi \simeq 0.3$, $E/E_0 \simeq 5.55, 5.6, 5.64, 5.66, 5.72$) all yielding strong spin-flipping transmissions with $0.9 \leqslant |I_\downarrow|$, with other TR coefficients being

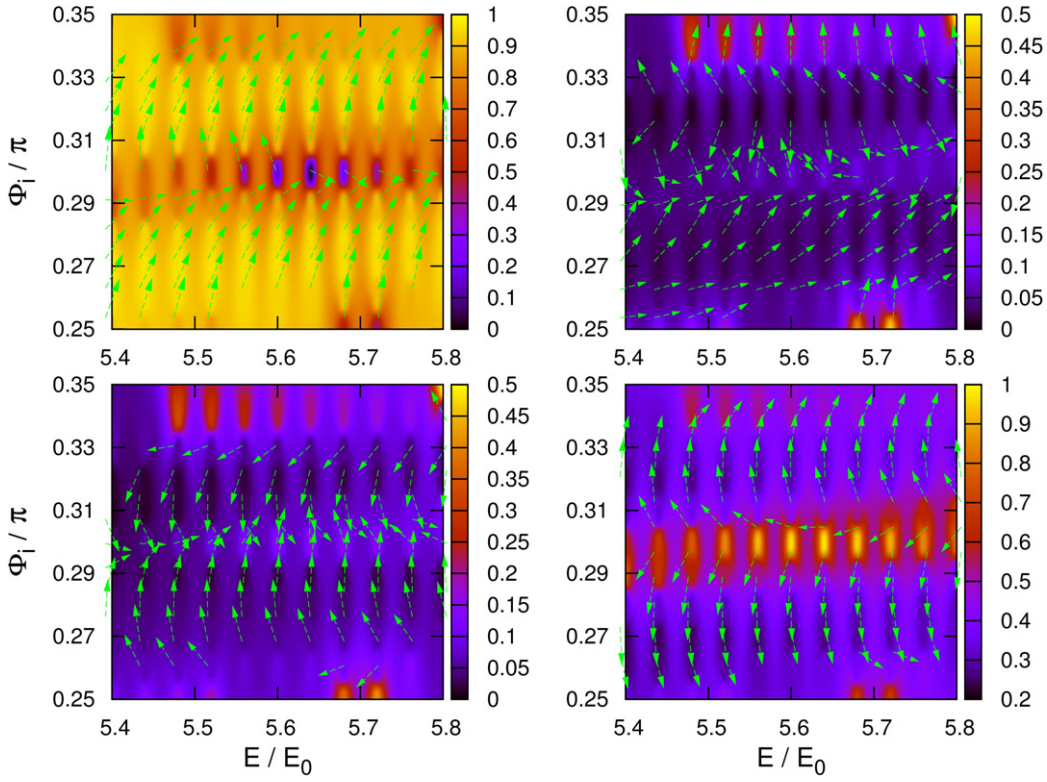

Figure 7. (Color online) The magnitudes and phases of the transmitted state against the parameters of incidence E/E_0, ϕ_i/π. Here $E_z/(150\ \mathrm{kV\ cm^{-1}}) = 1.6$, $V_\mathrm{P}/E_0 = 0.4$, $V_0/E_0 = 6$. The figures depict $(B_\uparrow, B_\downarrow, I_\downarrow, I_\uparrow)$, respectively, starting from the upper left corner in the counter-clockwise direction. The vertical boxes on the right of each figure indicate the magnitude of the reflection/transmission coefficients, and the counter-clockwise angle of the arrows with respect to the positive x direction is the phase of the respective amplitudes. In the calculations we assumed that the initial electron is spin-polarized in the $|\uparrow\rangle$ state.

much weaker. The phases of the corresponding transmission amplitudes are depicted by green arrows superimposed on the figure. The overall reference phase is the same in all plots. The phases of the TR amplitudes are strongly related to the $\phi_w^{(\pm)}$ via equation (5) and the boundary conditions. It is observed that the phase of the amplitudes has a weak dependence on the incident energies in the range $5.4 \leqslant E/E_0 \leqslant 5.8$ close to the barrier height but a strong dependence on the angle of incidence. These results are consistent with the weak dependence of $\phi_w^{(\pm)}$ in figures 3–5 on the incidence energy within the same range and a strong dependence on ϕ_i.

We now analyze one of these strongly spin-flipping resonances in figure 7 at ($\phi_i/\pi \simeq 0.3, E/E_0 \simeq 5.6$). The vicinity of this resonance is depicted in figure 8 as a function of the electric field and the plunger gate potential in the ranges $1.4 \leqslant E_z/(150\ \mathrm{kV\ cm^{-1}}) \leqslant 2.0$ and $0.2 \leqslant V_\mathrm{P} \leqslant 0.6$. The $\phi_i/\pi \simeq 0.3$, $E/E_0 \simeq 5.6$ resonance is confirmed here at $E_z/(150\ \mathrm{kV\ cm^{-1}}) \simeq 1.6$ and $V_\mathrm{P}/E_0 \simeq 0.4$. Additional resonances are observed in a closely spaced array as the electric field is changed within this range. The corresponding phases of the TR amplitudes are depicted by green arrows similarly to figure 7. Here we observe a stronger dependence of the phase of the amplitudes on E_z and V_P. These results are expected again within the scope of figures 3–5 where a strong dependence of $\phi_w^{(\pm)}$ is observed on V_P and E_z within the ranges $0.2 \leqslant V_\mathrm{P} \leqslant 0.6$ and $1.4 \leqslant E_z/(150\ \mathrm{kV\ cm^{-1}}) \leqslant 2.0$, respectively.

In this work, evidence is presented for externally controlling the spin-dependent refraction of an incident spin state traversing a medium with Rashba and Dresselhaus-type spin–orbit couplings. We considered a symmetric bar-shaped sample with a translational invariance in the y direction. As a result, the transmitted partial waves propagate in parallel directions. On the other hand, it is strongly desirable to angularly separate the transmitted partial amplitudes much like in Newton's optical prism. This is possible if the translational invariance is weakly broken by, for instance, a triangular geometry. If the size of the incident wave is much smaller than the lateral size of the device, the theoretical results presented here are unchanged and, as a bonus, it becomes possible to angularly separate the transmitted partial waves. Another important requirement for the device application is the independence of the diffraction angle from the energy of the incident electrons. This requirement is fulfilled if the incident energy of the particles is sufficiently large (lower right plots in figures 3–5). We also observe that spin-flipping processes are more efficient with a yield of nearly 100%, especially when the electron energy is close to the barrier height.

The controllable spin prism proposed here can also be examined for smaller QWs and different ranges of control parameters than studied here. The key here is the presence of the spin-independent resonant transmission states with sufficiently high energies. Under the SOC, those incident states which are within a certain neighborhood (determined

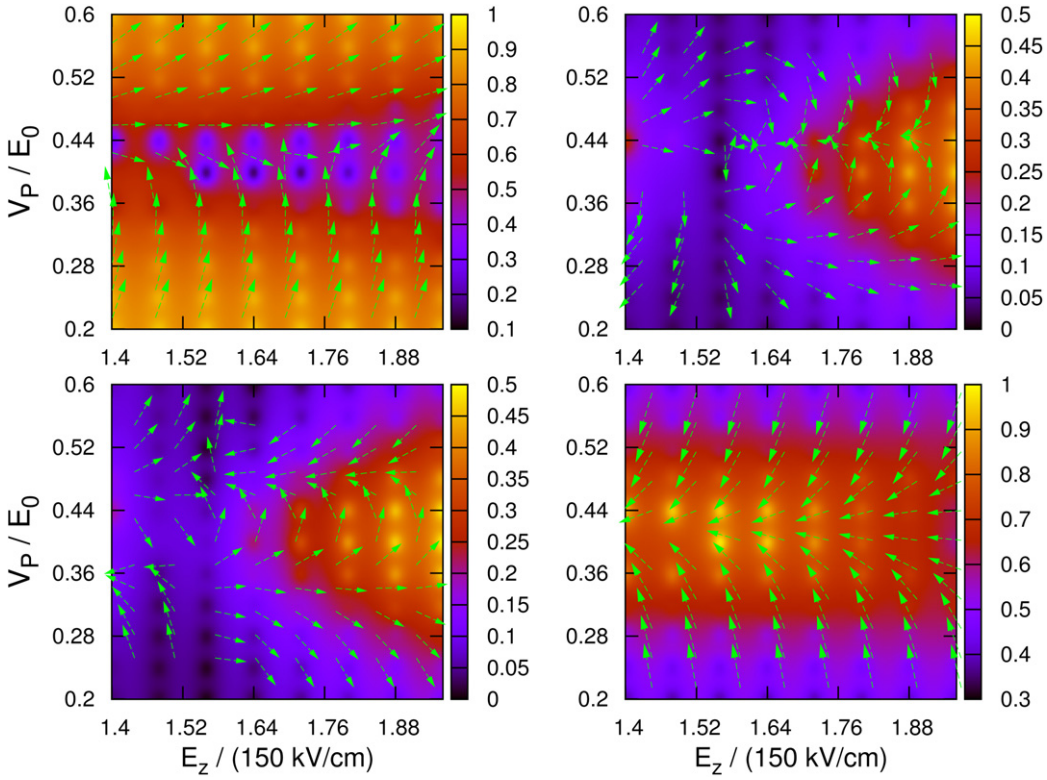

Figure 8. (Color online) The transmission magnitudes and phases against $E_z/(150\ \text{kV cm}^{-1})$ and V_P/E_0. Here $E/E_0 = 5.6$, $\phi_i = 0.3\pi$. The plots are in the same order as in figure 7.

by the SOC energy splitting) of the spin-independent resonant transmission energies are transmitted and their spin orientation is determined by the QW width as well as the strengths of the electric field and the plunger gate potential. An important point which is not included in our model is concerned with the presence of many electrons in the QW. The many-body Coulombic effects have been analyzed in the scope of the mean-field approximation by including the Coulomb effects in the form of a charging energy. It is found that [16] in the presence of nondegenerate levels (as in here) the presence of the charging energy in the QW shifts the position of the resonant peaks but also introduces an anomalous π-shift in the transmission amplitudes at the peak positions [17].

Yet another important constraint in the experimental feasibility of the device is concerned with the spin and momentum relaxation of the electrons due to the presence of electron–electron correlations, scattering off impurities and phonons. Due to the spin–orbit coupling present, the spin relaxation is strongly influenced by the momentum relaxation. There are detailed experimental results using high precision time-resolved absorption spectroscopy in the measurement of the spin relaxation times on the semiconductor heterostructures [19]. The experiments cover a large range of temperatures (4 K $< T <$ 300 K), electron energies (1 meV $< E <$ 140 meV) and sample widths (6 nm $< 2b <$ 20 nm). The experiments were also made in ambient conditions for the carrier density and found that the spin relaxation is not strongly dependent on the carrier concentration (see the third reference in [19]). In these materials the major source for spin relaxation is found from the quadratic temperature dependence of the spin relaxation rates to be a D'yakonov–Perel' mechanism [9, 19] at high temperatures, i.e. 10 K $\ll T$ and a Bir–Aharonov–Pikus mechanism at sufficiently low temperatures, i.e. $T \ll$ 10 K. The measured times vary from 10^{-2} to 1 ns (and even longer) depending on the temperature, the confinement energy, the electron concentration and the size of the QW. As the QW size decreases, the spin relaxation rate increases as a function of the confinement energy [19]. Combining the main results of these experimental works together we have that, in large undoped QWs, as considered in this work, and in the absence of magnetic field, the spin relaxation time is expected to be of the order of 500 ps at low temperatures ($T \lesssim 30$ K) which drops to about 200 ps at about $T = 100$ K (last reference in [19]). On the other hand, a typical electron dwelling time within the large inversion asymmetric medium in our model can be calculated for a typical electron density $n_e \lesssim 10^{11}$ cm^{-2} and the sample width $2b = 60$ nm to be of the order of 1 ps. These results indicate that the electron spin is far from relaxing even at room temperatures and high electron energies (less than the barrier height (35 meV in our case)) in scattering through such a tunneling device. As a result the electron wavefunction is expected to remain coherent. These conclusions may relax some of the experimental constraints on the operational conditions in the realization of these devices including those of the controllable spin prism studied here.

The results presented in this work may lead to further analogies with other linear optical and photonic devices. In this context, we can think of the spin analogs of lenses, partially

transmitting/reflecting mirrors, spin beamsplitters, as well as nanospheres, nanodiscs and nanorings. Hence, the controllable spin prism may stimulate experimental and theoretical work in a rich branch of spintronics device physics inspired by the linear optics and the photonics.

Acknowledgments

This research is funded by TÜBİTAK grant 105T110. The author thanks the Marmaris Institute of Theoretical and Applied Physics (ITAP) where parts of this work were produced. The figures were produced by GNUPLOT version 4.2.2. Discussion with S Mukhopadhyay is acknowledged.

References

[1] Datta S and Das B 1990 *Appl. Phys. Lett.* **56** 665
[2] Egues J C 1998 *Phys. Rev. Lett.* **80** 4578
Ohno H, Akiba N, Matsukura F, Shen A, Ohtani K and Ohno Y 1998 *Appl. Phys. Lett.* **73** 363
Ohno H 1998 *Science* **281** 951
Flatte M E, Yu Z G, Johnston-Halperin E and Awschalom D D 2003 *Appl. Phys. Lett.* **82** 4740
Kato Y, Myers R C, Gossard A C and Awschalom D D 2003 *Nature* **427** 50
Flatte M E and Vignale G 2001 *Appl. Phys. Lett.* **78** 1273
Johnston-Halperin E, Lofgreen D, Kawakami R K, Young D K, Coldren L, Gossard A C and Awschalom D D 2002 *Phys. Rev.* B **65** 041306
Zutic I, Fabian J and Das Sarma S 2002 *Phys. Rev. Lett.* **88** 066603
Fabian J, Zutic I and Das Sarma S 2004 *Appl. Phys. Lett.* **84** 85
Gregg J F 2001 *Spin Electronics* ed M Ziese and M J Thornton (Berlin: Springer)
[3] Rashba E I 1960 *Sov. Phys.—Solid State* **2** 1109
Bychkov Yu A and Rashba E I 1984 *JETP Lett.* **39** 78
Bychkov Yu A and Rashba E I 1984 *J. Phys. C: Solid State Phys.* **17** 6039
[4] Nitta J, Akazaki T, Takayanagi H and Enoki T 1997 *Phys. Rev. Lett.* **78** 1335
Egues J C, Burkard G and Loss D 2003 *Appl. Phys. Lett.* **82** 2658
Kiselev A A and Kim K W 2001 *Appl. Phys. Lett.* **78** 775
[5] Dresselhaus G 1955 *Phys. Rev.* **100** 580
[6] Schliemann J, Egues J C and Loss D 2003 *Phys. Rev. Lett.* **90** 146801
[7] Lusakowski A, Wrobel J and Dietl T 2003 *Phys. Rev.* B **68** 081201
Liu M-H and Chang C-R 2006 *Phys. Rev.* B **73** 205301
Saikin S, Shen M, Cheng M C and Privman V 2003 *Proc. Conf. IEEE-NANO 2003* vol 1 (Monterey, CA: IEEE) pp 91–4
[8] Citro R, Romeo F and Marinaro M 2006 *Phys. Rev.* B **74** 115329
Frustaglia D, Hentschel M and Richter K 2001 *Phys. Rev. Lett.* **87** 256602
Hatano N, Shirasaki R and Nakamura H 2007 *Phys. Rev.* B **75** 032107
Shen S-Q, Li Z-J and Ma Z 2004 *Appl. Phys. Lett.* **84** 996
[9] Zutic I, Fabian J and Das S S 2004 *Rev. Mod. Phys.* **76** 323
Wolf S A, Awschalom D D, Buhrman R A, Daughton J M, von Molnar S, Roukes M K, Chtchelkanova A Y and Treger D M 2001 *Science* **294** 1488
Prinz Gary A 1998 *Science* **282** 1660
[10] Khodas M, Shekhter A and Finkelstein A M 2004 *Phys. Rev. Lett.* **92** 086602
[11] Zhang X 2006 *Appl. Phys. Lett.* **88** 052114
[12] Sablikov V A and Tkach Y Ya 2007 *Phys. Rev.* B **76** 245321
[13] Meier L, Salis G, Shorubalko I, Gini E, Schön S and Ennslin K 2007 *Nat. Phys.* **3** 650
[14] Winkler R 2003 *Spin–Orbit Coupling Effects in Two-Dimensional Electron and Hole Systems* (Berlin: Springer)
[15] Winkler R 2000 *Phys. Rev.* B **62** 4245
[16] Hackenbroich G and Weidenmuller H A 1995 *Phys. Rev. Lett.* **76** 110
[17] Yacoby A, Heiblum M, Mahalu D and Shtrikman H 1995 *Phys. Rev. Lett.* **74** 4047
[18] Lee H-W 1999 *Phys. Rev. Lett.* **82** 2358
[19] Tackeuchi A, Nishikawa Y and Wada O 1996 *Appl. Phys. Lett.* **68** 797
Bar-Ad S and Bar-Joseph I 1992 *Phys. Rev. Lett.* **68** 349
Malinowski A, Britton R S, Grevatt T, Harley R T, Ritchie D A and Simmons M Y 2000 *Phys. Rev.* B **62** 13034
Britton R S, Grevatt T, Malinowski A, Harley R T, Perozzo P, Cameron A R and Miller A 1998 *Appl. Phys. Lett.* **73** 2140
Kikkawa J M and Awschalom D D 1998 *Phys. Rev. Lett.* **80** 4313